

Soft Matter

Accepted Manuscript



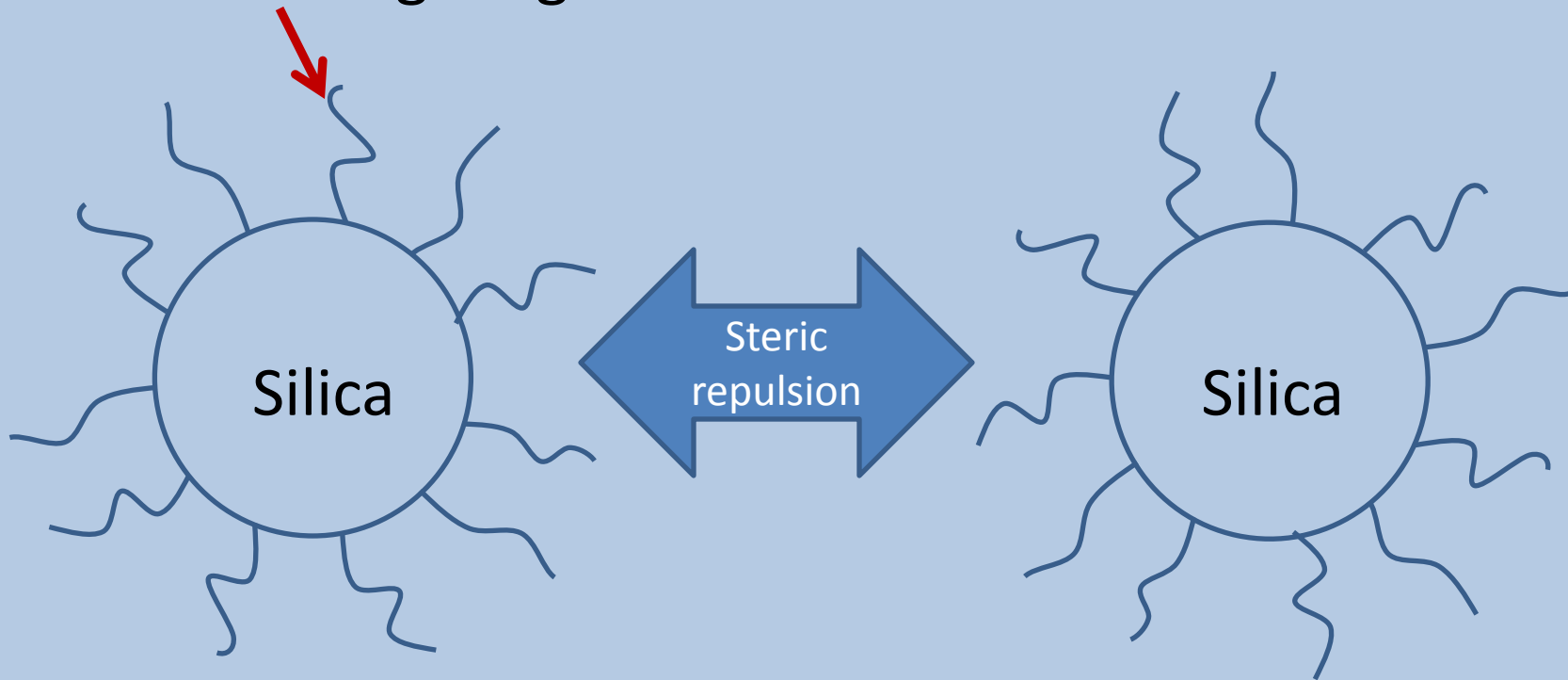
This is an *Accepted Manuscript*, which has been through the Royal Society of Chemistry peer review process and has been accepted for publication.

Accepted Manuscripts are published online shortly after acceptance, before technical editing, formatting and proof reading. Using this free service, authors can make their results available to the community, in citable form, before we publish the edited article. We will replace this *Accepted Manuscript* with the edited and formatted *Advance Article* as soon as it is available.

You can find more information about *Accepted Manuscripts* in the [Information for Authors](#).

Please note that technical editing may introduce minor changes to the text and/or graphics, which may alter content. The journal's standard [Terms & Conditions](#) and the [Ethical guidelines](#) still apply. In no event shall the Royal Society of Chemistry be held responsible for any errors or omissions in this *Accepted Manuscript* or any consequences arising from the use of any information it contains.

Low molecular weight ligands



High salinity brine

Steric stabilization of nanoparticles with grafted low molecular weight ligands in highly concentrated brines including divalent ions

Andrew J. Worthen, Vu Tran, Kevin A. Cornell, Thomas M. Truskett, and Keith P. Johnston*

McKetta Department of Chemical Engineering, University of Texas at Austin, Austin, Texas, USA

Keywords

Nanoparticle, stability, colloid, brine, ligand, steric stabilization, extended DLVO

Abstract

Whereas numerous studies of stabilization of nanoparticles (NPs) in electrolytes have examined biological fluids, the interest has grown recently in media with much higher ionic strengths including seawater and brines relevant to environmental science and subsurface oil and gas reservoirs. Given that electrostatic repulsion is limited at extremely high ionic strengths due to charge screening, we have identified ligands that are well solvated in concentrated brine containing divalent cations and thus provide steric stabilization of silica nanoparticles. Specifically, the hydrodynamic diameter of silica nanoparticles with grafted low molecular weight ligands, a diol ether, [3-(2,3-dihydroxypropoxy)propyl]-trimethoxysilane, and a zwitterionic sulfobetaine, 3-([dimethyl(3-trimethoxysilyl)propyl]ammonio)propane-1-sulfonate, is shown with dynamic light scattering to remain essentially constant, indicating lack of aggregation, at room temperature and up to 80°C for over 30 days. An extended DLVO model signifies that steric stabilization is strongly dominant against van der Waals attraction for ~10 nm particles given that these ligands are well solvated even in highly concentrated brine. In contrast, polyethylene glycol oligomers do not provide steric stabilization at elevated temperatures, even at conditions where the ligands are soluble, indicating complicating factors including bridging of the ether oxygens by divalent cations.

Introduction

Colloidal stability of nanoparticles (NPs) in aqueous media with high concentrations of electrolytes from biological fluids to seawater to even more concentrated brines is of scientific as well as

practical interest for many biomedical,¹⁻⁵ environmental,⁶⁻¹¹ and subsurface oil and gas¹²⁻¹⁷ applications. In rapidly advancing imaging^{12, 16, 18, 19} and oil recovery²⁰⁻²² applications of NPs in subsurface oil and gas reservoirs,²³ the concentration of monovalent and divalent ions is extremely high, on the order of several weight percent and up to 22% total dissolved salts in certain applications.²⁴ According to DLVO theory,^{6, 25} van der Waals forces will often cause aggregation of NPs in concentrated brine since high screening of the charges on the particles weakens electrostatic repulsion markedly. For example, the Debye screening length is only 0.9 nm at an ionic strength of 150 mM in blood, 0.4 nm at 600 mM in seawater, and 0.2 nm at 1.7 M encountered in subsurface reservoirs (i.e. API brine with 8% NaCl and 2% CaCl₂). For systems containing Ca²⁺ and/or other divalent ions, interparticle bridging attraction with anions on the particle surfaces, such as carboxylate groups can contribute strongly to aggregation.^{26, 27} At the critical coagulation concentration (CCC) of an electrolyte, aggregation becomes diffusion controlled and very rapid, as described by Smoluchowski.²⁸⁻³² For NaCl, the CCC is on the order of 400 mM at pH 10 for 15-25 nm diameter silica nanoparticles.^{32, 33} For symmetric electrolytes, the CCC is inversely proportional to the sixth power of the valence according to the Schulze-Hardy rule.²⁹ For the Derjaguin approximation in the limit as $\Psi_0 \rightarrow \infty$, the predicted CCC is ~100 fold smaller for an asymmetric 2:1 electrolyte such as CaCl₂ than a 1:1 electrolyte.²⁹ In agreement with this prediction, the CCC for 30 and 60 nm Ag nanospheres coated with citrate decreases by ~100 fold to 2.1 mM for CaCl₂ relative to NaCl.^{34, 35} Since this electrolyte concentration is orders of magnitude smaller than those encountered in each of the aqueous media of interest in this study, it will be necessary to provide steric stabilization to prevent coagulation.

According to the classic concept developed by Napper,³⁶ a ligand attached to the surface may provide steric stabilization when it is sufficiently well solvated to be soluble in the solvent.^{28, 36} For example, hexanethiol ligands are soluble in supercritical water at 400°C and 200 bar at low salinities and stabilize copper nanoparticles.³⁷ For the case of concentrated brines with ionic strengths above ~300 mM, particularly those containing divalent ions, relatively few ligands are soluble at room temperature, and even fewer at elevated temperatures. Adsorbed surfactant bilayers have been used to disperse 3 nm CdSe quantum dots at salinities up to seawater and at temperatures up to 60°C (below the surfactant cloud point of 70°C),³⁸ but have not been demonstrated for larger particles. The current state of the art for stabilizing ca. 10 to 100 nm nanoparticles in high salinity brines is to adsorb^{18, 19, 39-41} or graft^{12, 16, 42-44} polymer chains onto the nanoparticle surfaces to provide steric (or electrosteric) stabilization. In seawater, copolymers containing styrene sulfonate have been found to stabilize 40 nm

iron oxide nanoparticles,⁴⁵ and the homopolymer poly(allylamine) to stabilize 20 nm silver NPs.⁴⁶ At higher salinities, polymer coatings containing sulfonate groups such as 2-acrylamido-2-methylpropane sulfonic acid (AMPS)^{18, 47} or sulfobetaines^{16, 42} have been shown to stabilize ca. 100 nm diameter iron oxide nanoparticles in API brine (8% NaCl + 2 % CaCl₂) at 90°C for at least 30 days. For AMPS where Ca²⁺ ions bind very weakly to the sulfonate group, the charged polymer chains remain hydrated and extended, even up to 90°C and provide electrosteric stabilization.^{12, 18, 42, 48, 49} Conversely, polyelectrolytes which bind strongly to cations tend to be poorly solvated in brine and thus ineffective.^{18,}

36

To our knowledge, steric stabilization of nanoparticles in seawater or more concentrated brines with high divalent concentrations has not been reported with a well-defined grafted monomeric low molecular weight ligand (< ca. 1 kDa). This limitation is a consequence of the lack of solvation of most ionic or nonionic ligands in concentrated brines containing divalent ions.³⁶ In contrast, electrolytes are commonly used to aggregate nanoparticles to form clusters by screening electrostatic repulsion or by bridging attraction with divalent ions.^{50, 51} For NPs greater than 100 nm in diameter, oligomeric or polymeric ligands are usually required to provide a sufficient range of steric repulsion to counterbalance van der Waals (vdW) attraction.³⁶ In contrast, very short monomeric ligands may be sufficient to overcome this attraction for NPs smaller than 10 nm where vdW attraction is weaker. A few examples of stable NPs have been reported in brines containing concentrated monovalent ions, particularly NaCl, where ligands are more readily solvated than in the case of divalent ions. Small NPs with monomeric zwitterionic sulfobetaine ligands^{2, 4, 52, 53} have been demonstrated to be stable at high salinity conditions, for example sulfobetaine-coated silica NPs were stable at room temperature in 3 M NaCl for 15 days,⁴ and sulfobetaine-coated CdSe/ZnS quantum dots had at least limited colloidal stability in saturated NaCl brine (~6 M NaCl).² Additionally, silica NPs coated with 6-9 repeat unit poly(ethylene glycol) (PEG) were found to be stable in 3 M NaCl at room temperature for 24 h⁵ and silica NPs coated with “short-chain” PEG of unknown molecular weight (MW) were found to be stable in 8% NaCl at up to 50°C,²¹ but divalent ions were not included in either study. Whereas PEG chains with molecular weights greater than 1 kDa are well known to become insoluble in brines at elevated temperatures,⁵⁴ their solubility increases with a decrease in MW.⁵⁵ In the current study however, we were unable to stabilize NPs in API brine above about 50°C with low molecular weight PEG ligands. Gold nanoparticles with thymine oligomers with 5 repeat units were stable in seawater for up to 9 days at room temperature,⁵⁶ but to our knowledge monomeric biological molecules such as amino acids and nucleobases have not yet been demonstrated to stabilize NPs in seawater or brines containing concentrated divalent cations. A highly

salinity-tolerant carbon-based nanoparticle was developed by Giannelis and coworkers⁵⁷ which is of interest as a tracer particle to track flow in oil reservoirs. However, the particle's surface, believed to contain polar ethoxy groups produced during particle synthesis,⁵⁷ is not well defined. Given the current state of knowledge, a major challenge will be to identify new low MW ligands that are sufficiently well solvated to be soluble in concentrated brines containing divalent ions and can be grafted to NP surface to provide steric stabilization.

The objective of this study was to identify low MW ligands that are solvated and thus stabilize 7 to 20 nm silica nanoparticles in concentrated brines with high levels of divalent ions (seawater and API brine) at ambient and elevated temperatures. The NPs we investigate are shown to be stable against aggregation up to 80°C for over 30 days in API brine, as measured by dynamic light scattering. We contrast the behavior for three types of nonionic ligands, a diol ether ([3-(2,3-dihydroxypropoxy)propyl]-trimethoxysilane, GLYMO) and ethylene glycol oligomers with an average number of repeat units of either 6-9 (methyl terminated) or 8-12 (hydroxyl terminated) with that for a zwitterionic sulfobetaine, 3-[[dimethyl(3-trimethoxysilyl)propyl]ammonio]propane-1-sulfonate (SB). GLYMO and SB are each shown to provide colloidal stabilization of NPs in seawater and API brine with concentrated divalent ions, an elusive goal that has not been reported previously for any low molecular weight ligand to our knowledge. Highly versatile silylation chemistry is used to attach covalently each ligand to the surface of pre-synthesized silica NPs. Although GLYMO has been shown to provide steric stabilization of silica in water,⁵⁸ the behavior was not investigated in brine. In the case of zwitterionic ligands, added electrolytes screen the attraction between the strong dipoles and raise the solubility, known at the "antipolyelectrolyte effect".^{1,3} An extended DLVO approach is used to show that the low MW ligands are long enough to provide steric stabilization given sufficiently favorable Flory-Huggins interaction parameters, despite the high level of electrostatic screening in API brine. We hypothesize that the nonionic or zwitterionic stabilizing ligand "buries" a significant fraction of the anionic charges (deprotonated silanols) on the bare silica surface to mitigate interparticle bridging of these charges with Ca²⁺ ions. The greater stabilization at high temperatures with the diol ether GLYMO relative to ethylene oxide oligomers is explained in terms of the greater hydrophilicity of the former and much stronger bridging of Ca²⁺ to the ethylene oxide groups than the diols.

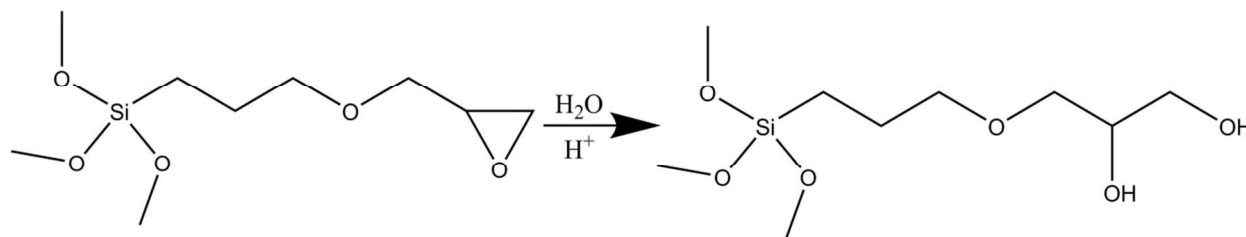
Experimental

Materials. Spherical colloidal silica nanoparticles were purchased from Nyacol Nano Technologies (NexSil 6, 12, 20, and 125) or received as a gift from Nissan Chemical Company (Snowtex PS-S, UP, and

O). Silylating agents containing 6-9 EO units (2-[methoxy(polyethyleneoxy)6-9propyl]trimethoxysilane, PEG(6-9EO), 90%, Cat. No. SIM6492.7), 8-12 EO units ([hydroxyl(polyethyleneoxy)propyl]triethoxysilane, PEG(8-12EO), 50% in ethanol, Cat. No. SIH6188.0), or sulfobetaine (3-([dimethyl(3-trimethoxysilyl)propyl]ammonio)propane-1-sulfonate, SB, 95%, Cat. No. SID4241.0) were purchased from Gelest (see Figure 1, upper for structures). (3-glycidyloxypropyl)trimethoxysilane ($\geq 98\%$, Sigma-Aldrich), HCl (1N solution, Fisher Scientific), NaOH (1N solution, Fisher Scientific), NaCl (ACS Grade, Fisher Scientific), $\text{CaCl}_2 \cdot \text{H}_2\text{O}$ (ACS Grade, Amresco), triethylene glycol (TEG, 99%, Acros Organics), and synthetic seawater (SSW, Cat. No.8363-5, Lot 1306873, ASTM D1141, pH 8.2, Ricca Chemical Co.) were used as received. Deionized (DI) water (Nanopure II, Barnstead, Dubuque, IA) was used for all experiments.

Specific surface area measurement. The pH of silica nanoparticle dispersions was first lowered to approximately 3 by mixing with H^+ ion exchange resin (Dowex Marathon C, Sigma-Aldrich) to remove excess Na^+ ions. The dispersion was then decanted into a petri dish and dried at 120°C overnight to remove water. The dried sample was finely ground using an agate mortar and pestle before performing Brunauer, Emmett, and Teller (BET) surface area measurements through nitrogen sorption on a Quantachrome Instruments NOVA 2,000 high-speed surface area BET analyzer at a temperature of 77 K. The measured specific surface areas of bare silica NPs are given in Table S1.

Synthesis of GLYMO-coated silica. The synthesis of GLYMO-coated silica nanoparticles was based on that of previous studies.^{4, 58} An aliquot of (3-glycidyloxypropyl)trimethoxysilane (typically 0.51 mL for a 1 g batch of NexSil 6 particles) was added to 0.01 M HCl (pH = 2) (typically in a ratio of 1:6 by volume) and stirred for 2 minutes at room temperature to perform acid-catalyzed ring opening shown in Scheme 1 to form GLYMO.⁵⁹



Scheme 1. Ring opening of (3-glycidyloxypropyl)trimethoxysilane to form GLYMO.

The solution rapidly turned from turbid to clear as the reaction proceeded due to the high solubility of the GLYMO product and low solubility of the (3-glycidyloxypropyl)trimethoxysilane reactant.

The resulting solution of GLYMO starting material (shown in Scheme 1 and Figure 1, upper) was immediately added dropwise to a vial containing nanoparticles and DI water such that the final concentration of nanoparticles was 10% (w/v). The amount of GLYMO added was varied from 0.1 to 10 $\mu\text{mol GLYMO}/\text{m}^2$ of silica nanoparticle surface (determined by BET) to achieve various GLYMO coverages on the nanoparticles. The reaction pH was increased to 10 with concentrated NaOH and the solution was stirred for 24 h at 60°C. A variation of the aforementioned procedure was used for one batch of NexSil 6 + GLYMO (denoted with a “*”), where half of the GLYMO was added to the reaction mixture and stirred at room temperature for 2 h, then the second half of the GLYMO was added and the mixture was stirred at 60°C for an additional 22 h. We note that the silica NPs are expected to be chemically stable at pH 10, but they are expected to dissolve above ca. pH 11.⁶⁰

After 24 h of reaction time, the dispersion was washed four times with DI water using 30k MWCO centrifuge filters at 5500 rpm for 15 minutes to remove ungrafted ligands and reaction byproducts. After the final filtration, DI water was added to the retentate to bring the concentration to ca. 10% w/v silica NPs. The dispersion was bath sonicated for 15 min. and passed through a 0.45 μm syringe filter to remove any large aggregates that might have formed during the purification process. An aliquot of the dispersion was dried overnight at 80°C to determine the final concentration of silica + GLYMO coating in the dispersion. The NP concentrations in this manuscript are given in terms of total mass of solids in the dispersion (i.e. total mass of silica particles + grafted ligands).

Grafting of PEG(8-12EO) to silica NPs. To avoid aggregation of silica nanoparticles by the ethanol in the PEG(8-12EO) stock solution, two approaches were used. First, Snowtex O nanoparticles were used in the synthesis due to their resistance to aggregation in the presence of ethanol. For this sample, the PEG(8-12EO) stock solution was dissolved in DI water in a ratio of 1:1 by volume. This solution was immediately added dropwise to a diluted Snowtex O nanoparticle dispersion such that the final concentration of silica was 10% w/v. The grafting reaction and subsequent purification were then performed as in the GLYMO grafting procedure given above.

A second approach was used to graft PEG(8-12EO) to NexSil 6 particles to prevent aggregation that was observed for high concentrations of ethanol in solution. To remove ethanol from the PEG(8-12EO) stock solution to avoid this particle aggregation during the grafting step, an aliquot necessary to provide 5 $\mu\text{mol PEG(8-12EO)}/\text{m}^2$ of silica nanoparticle surface was added to TEG in a 1:1 ratio by volume and stirred overnight in an open vial at 90°C. After this process, the volume of the solution decreased by approximately 25%, primarily due to the evaporation of ethanol. The resulting silane-in-TEG solution

was added dropwise to diluted NexSil 6 nanoparticle dispersion such that the final concentration of silica was 10% w/v and the added silane was sufficient to provide 5 $\mu\text{mol coating}/\text{m}^2$ of silica nanoparticle surface. The grafting reaction and subsequent purification were then performed as in the GLYMO grafting procedure given above.

Grafting of SB or PEG (6-9EO) to silica NPs. An aliquot necessary to provide 5 $\mu\text{mol coating}/\text{m}^2$ of silica nanoparticle surface of SB or PEG (6-9EO) was dissolved in DI water in a ratio of 1:6 by volume. This solution was immediately added dropwise to a nanoparticle dispersion such that the final concentration of silica was 10% w/v. The grafting reaction and subsequent purification were then performed as in the GLYMO-coated silica. A GLYMO grafting step was attempted on some SB-coated NPs (denoted by “***”), where the SB-coated particles were used in place of bare silica particles in the GLYMO grafting procedure detailed above.

Dynamic light scattering (DLS). Hydrodynamic diameters were measured with a Brookhaven ZetaPALS instrument with the BI-MAS configuration. Scattered light was collected at 90° with an Avalanche photodiode detector, and all data were fit with the NNLS routine using an autofit to 12 channels. The NP concentration was adjusted to give a count rate of ca. 500 kcps. All measurements were made over a period of 1 min. and in triplicate, where the average and standard deviation of the three runs was recorded.

Zeta potential. Zeta potentials were calculated with the Smoluchowski model from electrophoretic mobilities of silica nanoparticles measured at room temperature in disposable zeta cells (DTS 1070) with a Malvern Zetasizer Nano ZS or Brookhaven ZetaPALS (as indicated). The settings of the instrument were checked by measuring a standard latex particle sample with a zeta potential of -68 ± 5 mV. All particle concentrations were 0.5% w/v and the pH was adjusted with concentrated NaOH or HCl at least 1 hour prior to measuring the zeta potential. A background electrolyte of 10 mM NaCl (Malvern) or 10 mM KCl (Brookhaven) was used in all measurements. Samples were run in triplicate, where the average and standard deviation of the three runs was recorded.

Determination of ligand grafting density. The organic content of surface-modified silica NPs was determined through thermogravimetric analysis (TGA) using a Mettler-Toledo TGA/SDTA851e instrument. Before loading the sample into the instrument, it was dried overnight at 80°C in a convection oven. The sample was then heated under N_2 at 20°C/min in the TGA instrument from room temperature to 110°C and held for 20 minutes to remove remaining water. The organic fraction (W_o)

was recorded as the fractional weight lost under an atmosphere of air at from 110°C to 800°C, heating at a rate of 20°C/min. The ligand grafting density (μm^2 ligand/ m^2 of nanoparticle surface) was calculated from W_0 with the known “effective” molecular weight of the ligand (Table S2) and particle specific surface area (Table S1). Note that the “effective” molecular weight of the ligand was calculated by excluding the methyl or ethyl groups (which are lost prior to the TGA measurement due to hydrolysis during the grafting step) and the silicon or oxygen atoms (which are not lost in the TGA due to the strength of the Si-O-Si bond holding the ligand to the particle surface). A complete monolayer of grafted ligand was assumed to be $7.6 \mu\text{m}^2$ of nanoparticle surface, based on 4.6 SiOH groups / nm^2 as available grafting sites.⁶⁰ Further details are given in the Supporting Information to describe the calculations of the monolayer fractions.

Transmission electron microscopy (TEM). TEM experiments were performed on a FEI TECNAI G2 F20 X-TWIN TEM instrument. A dilute aqueous dispersion of the IO nanoclusters was deposited onto a 200 mesh carbon-coated copper TEM grid and allowed to dry overnight at ambient conditions before imaging.

Solid-state ^{13}C (^1H) CP MAS NMR. The solid-state ^{13}C (^1H) CP MAS NMR spectra were obtained with a Bruker solid-state NMR spectrometer Avance-400 (400 MHz for ^1H) equipped with a standard 4 mm or 2.5 mm MAS probe head, as indicated. The MAS NMR spectra have been recorded with a standard cross-polarization pulse sequence at relaxation delays of 5 s and a spinning rate of 10 kHz. The ^{13}C chemical shifts are reported relatively to TMS as an external reference. The total experimental time is 24 h or 12 h, as indicated. The resulting signal:noise ratio was improved when the experimental time was 24 h (as shown in the following section for GLYMO-coated NPs). However, even with the greater noise in the 12 h experiments the chemical species on the NPs could be identified, as only qualitative results were needed.

Nanoparticle stability determination. Nanoparticle dispersions at a concentration of 0.5% w/v were diluted in either (1) SSW or (2) NaCl and/or CaCl_2 solutions to a final salt concentration of either 0.5% NaCl or 8% NaCl + 2% CaCl_2 (API brine). The pH was left unadjusted (pH 8~9) or adjusted to 3.5 with 1N HCl. Samples were then stored either at room temperature ($23\pm 1^\circ\text{C}$) or in a convection oven at 80°C or 120°C NP sizes were measured over time by DLS up to at least 720 h (30 d) if the sample remained colloidally stable, and visual observations of nanoparticle dispersions were also recorded. Detailed characterization of NP stability past 720 h was beyond the scope of the present study, but limited data are given where available. The critical flocculation temperature (CFT) of PEG-coated silica nanoparticles

was recorded by increasing the temperature of a 2 mL aliquot of NP dispersion in a glass vial with a stirred oil bath. The temperature and visual observations were simultaneously recorded. The CFT was recorded as the temperature at which the sample became visually turbid.

Dispersion rheology. The steady-state shear rheology of aqueous dispersions of NPs was measured at 25°C using a AR G2 rotational rheometer (TA Instruments) with a concentric cylinder geometry (14 mm radius x 42 mm height, part # 546012.901).

Extended DLVO approach to calculate interparticle interactions. According to extended DLVO theory, the total potential between two spherical particles with radius R at a particle separation of h may be written as the sum of the van der Waals (V_a), electrostatic (V_r), and steric (V_s) potentials,

$$V_t(h) = V_a(h) + V_r(h) + V_s(h) \quad (1)$$

The van der Waals potential

$$V_a(h) = -\frac{(R+L)(A_m^{0.5} - A_p^{0.5})^2}{12 \cdot h} \quad (2)$$

where L is the thickness of the particle coating, A_m and A_p are the Hamaker constants for the medium and particle, respectively.⁶¹ Note that the coating material is assumed to have the same Hamaker constant as the core particle to give a conservatively high estimate of V_a , and thus the sum of the particle radius and coating thickness is considered for this calculation. The electrostatic potential V_r

$$V_r(h) = 2 \cdot \pi \cdot R \cdot \varepsilon_0 \cdot \varepsilon_r \cdot \psi_0^2 \ln[1 + \exp(-\kappa \cdot h)] \quad (3)$$

where ε_0 is the permittivity of vacuum, ε_r is the relative permittivity of the electrolyte solution, ψ_0 is the surface potential and κ is the Debye screening parameter length given by

$$\kappa = \left(\frac{2N \cdot e^2 \cdot I}{\varepsilon_0 \cdot \varepsilon_r \cdot k_B \cdot T} \right) \quad (4)$$

where N is the Avogadro number, e is the elementary electric charge, and I is the ionic strength of the electrolyte solution.⁶² Note that only the core particle is considered to have a significant contribution to the overall particle charge and thus only the core particle radius is considered for this calculation.

The steric repulsion potential V_s for the grafted ligands was calculated by summing the contributions of osmotic (V_o) and entropic/elastic (V_e) effects based on a model introduced by Vincent et al.⁶³ that has been used for both polymeric⁶⁴ and low molecular weight⁶⁵ ligands,

$$V_s(h) = V_o + V_e \quad (5)$$

The overlap of the steric layers on two approaching nanoparticles results in increased osmotic pressure in the overlap region and thus repulsion V_o between the particles, represented by the piecewise function

$$\begin{aligned} V_o &= 0 & 2L \leq h \\ V_o &= \frac{4\pi R}{v_1} \phi^2 \left(\frac{1}{2} - \chi \right) \left(L - \frac{h}{2} \right)^2 & L \leq h < 2L \\ V_o &= \frac{4\pi R}{v_1} \phi^2 \left(\frac{1}{2} - \chi \right) L^2 \left(\frac{h}{2L} - \frac{1}{4} - \ln \left(\frac{h}{L} \right) \right) & h < L \end{aligned} \quad (6)$$

where χ is the Flory-Huggins interaction parameter, ϕ is the volume fraction of ligand in the coating layer, and v_1 is the volume of one solvent molecule. Compression of the ligands beyond $h = L$ leads to a loss of entropy for the ligands, giving rise to entropic/elastic repulsion V_e between the particles, represented by the piecewise function

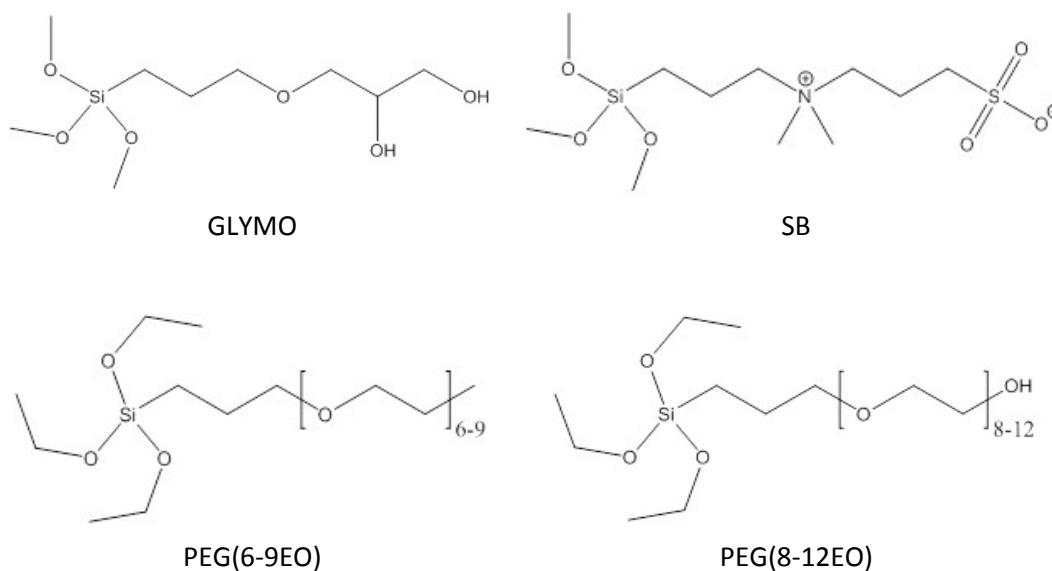
$$\begin{aligned} V_e &= 0 & L \leq h \\ V_e &= \frac{2\pi R}{M_w} \phi L^2 \rho_p \left[\frac{h}{L} \ln \left(\frac{h}{L} \left(\frac{3-h/L}{2} \right)^2 \right) - 6 \ln \left(\frac{3-h/L}{2} \right) + 3 \left(1 + \frac{h}{L} \right) \right] & h < L \end{aligned} \quad (7)$$

where M_w is the molecular weight of the ligand and ρ_p is its bulk density. The parameters used for DLVO calculations are given in Table S3. We caution that the calculations presented in this study are only semi-quantitative due to the inherent assumptions in the models⁶⁶ and thus the results are given for comparison rather than prediction. For example, the potentials estimated above include the Derjaguin approximation, which is only valid for separations much smaller than the diameter of the particles and includes a continuum assumption which is only valid at values of h larger than the molecular length scale of the solvent and ions in solution.⁶⁶ Nevertheless, the calculations highlight the important role of grafted ligand for NP stability in brine.

Results and Discussion

The results and discussion section begins with characterization of the grafted nanoparticles and then presents the colloidal stability in the high salinity aqueous phases. The stability data are then analyzed with an extended DLVO model to describe the stabilization mechanisms.

Phase behavior of the ligands in API brine. The structures of the four low molecular weight ligands are given in Figure 1. Remarkably, all were soluble at 0.05 %w/v in API brine up to 120°C at pH 7±1 (Figure S4, where images were taken less than 30 s after removal from the 120°C oven), and thus according to the concept of Napper,³⁶ are candidates for steric stabilization. Furthermore, 300 Da PEG (ca. 6 repeat units) was soluble for concentrations up to 30 %w/v indicating the temperature was still below the lower critical solution temperature (LCST) (Figure S4). For the PEG oligomers, the low molecular weight was necessary to remain below the LCST as the LCST is known to increase with a decrease in MW.⁵⁵ For example, 300 Da PEG is soluble in API brine at up to 120°C, whereas 8 kDa PEG is insoluble at the same conditions (Figure S4). Similar behavior is known for PEG ethers; the lower critical solution temperature of the water/ethylene glycol n-butyl ether system is 48°C, and it drops to 40°C for water/diethylene glycol n-pentyl ether.⁶⁷



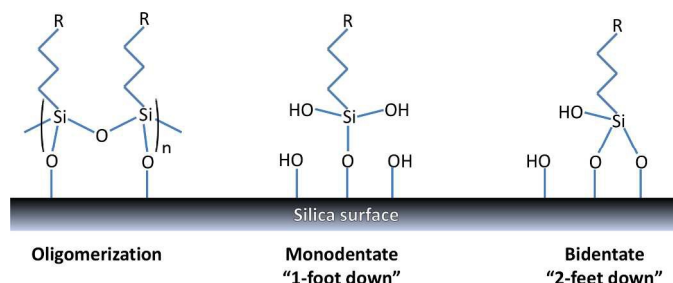


Figure 1. Upper: structures of silylating agents. Lower: Various configurations of silylating agents on a silica surface (Adapted from Estephan 2010).

Nanoparticle characterization. Table 1 summarizes the properties of the various silica particles investigated in this study, before and after grafting with stabilizing ligands. The NexSil series of particles are spherical with hydrodynamic diameters (D_h s) from ca. 7.4 to 104 nm while the Snowtex (ST) particles are elongated aggregates of primary NPs. Photographs of the NP dispersions are given in Figure 2, TEM in Figure 3, and representative DLS size distributions in Figure S2. The larger 12 and 124 nm NPs scattered more light and appeared more turbid at a given concentration than the smaller 7.4 nm NexSil 6 (Figure 2). As summarized in Table 1, the D_h of the small NexSil 6 particles increased in some cases from 7.4 nm to ca. 20 nm after grafting, due to a small degree of particle aggregation during synthesis. The aggregation was evidenced by the increased width of the DLS size distributions given in Figure S2, especially in the case of NexSil 6 + SB NPs (Figure S2d) which had a lower ligand coverage than the GLYMO-coated NPs. These results suggest that higher ligand coverages can prevent aggregation during synthesis (see also Figure S8b for various GLYMO ligand coverages on NexSil 6 NPs where NPs with higher ligand coverage underwent less aggregation). The aggregation is also evident by TEM for NexSil 6 + GLYMO in Figure 3b. When GLYMO was added in two portions (denoted by “*”), the D_h increased to only 9.6 nm, indicating very minimal aggregation (Table 1 and Figure 3a). This smaller D_h may suggest reduced inter-particle bridging given less oligomerization of the ligands during formation of Si-O-Si bonds. For the non-spherical ST-PS-S and ST-UP particles, two characteristic D_h s were observed by DLS, which did not significantly change after grafting (Table 1). The larger D_h size was likely due to translational diffusion and the smaller due to rotational diffusion;⁶⁸ however, polydispersity in aggregate size will also contribute to the distribution. For the GLYMO-coated NexSil-series particles, a clear trend of decreasing organic fraction with increasing core particle size was observed, as expected, given the lower surface area to volume ratio of larger particles. The organic fraction of PEG-coated particles was expectedly higher than for GLYMO-coated particles of the same size given its higher molecular weight.

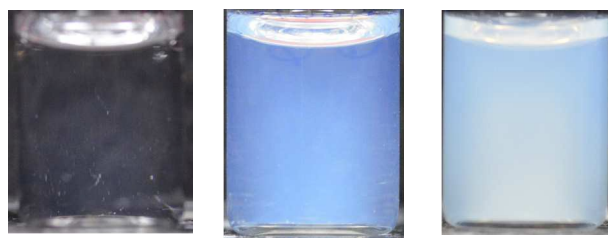
The calculated coverages of the coatings indicate that 11 to 64% of a ligand monolayer of ligand was present in all cases, in agreement with previous experiments with other short ligands grafted to silica via silylation chemistry.⁴

Table 1. Properties of grafted nanoparticles and critical flocculation temperatures in SSW and API brine

NP Core	Core particle D_h in DI @ RT, nm	Ligand	Grafted particle D_h in DI @ RT, nm (TEM size, nm)	Particle organic fraction by TGA, wt.%	Ligand coverage, $\mu\text{mol}/\text{m}^2$ (monolayer fraction)	CFT in SSW, pH~8, 0.5% w/v NPs, °C	CFT in API, pH~8, 0.5% w/v NPs, °C
NexSil 6	7.4±0.4	GLYMO*	9.6±1.5 (9.9±2.0)	11.7	2.7 (35%)	√	√
NexSil 6	7.4±0.4	GLYMO	16.5±2.3 (12.9±2.8)	13.8	2.9 (38%)	√	√
NexSil 12	21.0±4.4	GLYMO	31.3±1.7 (21.6±4.0)	8.0	3.3 (43%)	√	√
NexSil20	24±1.7	GLYMO	20.7±0.9 (28.6±7.0)	5.6	3.8 (49%)	√	√
NexSil125	104±12	GLYMO	93.9±6.5	3.1	4.9 (64%)	√	√
ST-PS-S	21.4±8.3 and 128±6	GLYMO	23.9±2.8 and 159±13	8.8	4.1 (54%)	√	√
ST-UP	20.9±4.8 and 86.0±12.8	GLYMO	12.5±1.4 and 79.1±14.0	8.9	3.2 (42%)	√	√
NexSil 6	7.4±0.4	SB	24.2±3.5	12.5	1.7 (22%)	√	√
NexSil 6	7.4±0.4	SB**	20.9±2.2 (11.1±2.5)	12.1	1.6 (21%)	√	√
NexSil 6	7.4±0.4	PEG (6-9EO)	18.0±2.7	26.0	2.1 (28%)	81 [‡]	49 [‡]
NexSil 6	7.4±0.4	PEG (8-12 EO)	19.6±1.2	15.3	0.9 (11%)	85	50

[‡]Re-disperses when cooled

√ = no CFT observed up to 95°C



(a)

(b)

(c)

Figure 2. Photographs of 0.5% (a) NexSil 6 + GLYMO*, (b) NexSil 12 + GLYMO, and (c) NexSil 125 + GLYMO in DI water right after forming the dispersions. Note the increasing turbidity with increasing particle diameter (images taken in front of dark grey background). Vial outside diameter = 1.47 cm.

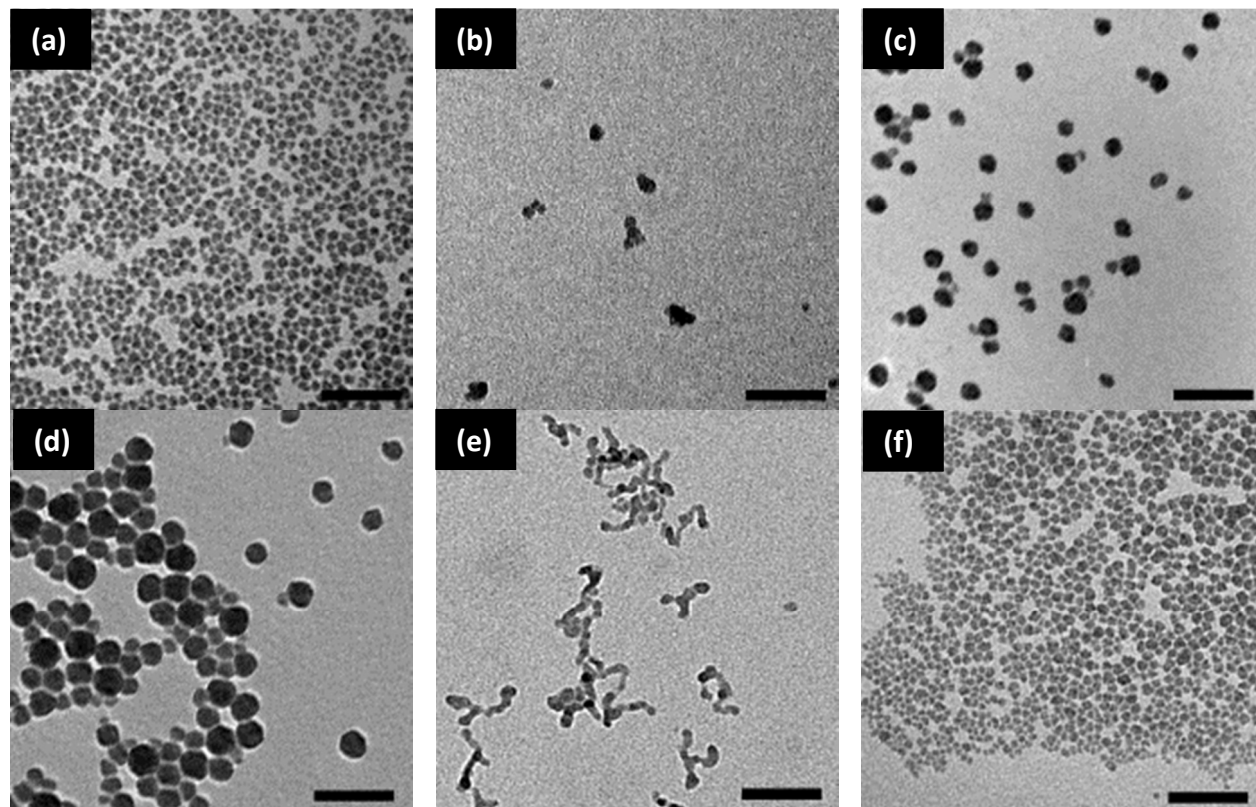


Figure 3. TEM images of (a) NexSil 6 + GLYMO*, (b) NexSil 6 + GLYMO, (c) NexSil 12 + GLYMO, (d) NexSil 20 + GLYMO, (e) ST-UP + GLYMO, (f) NexSil 6 + SB**. Scale bars are 100nm.

Figure 4 shows ^{13}C (^1H) CP MAS NMR spectra for the four ligands used in this study. The spectrum for bare silica particles (not shown) did not indicate any carbon signals above the noise level, indicating carbon-containing impurities were not present in the bare NP samples. All spectra of the grafted NPs shown in Figure 4 are consistent with the structures of the ligands. For GLYMO-coated silica NPs (Figure 4a), the location of the peaks for carbons 1-4 are in good agreement with literature for the unreacted epoxide.⁵⁹ After the opening of the epoxide ring (Scheme 1), the peaks for carbons 5 and 6 shift from around 50 and 45 ppm, respectively,⁵⁹ to 55.7 and 63.2 ppm. The absence of peaks in the 40-50 ppm range in Figure 4a indicates unreacted epoxide was not present indicating complete formation of GLYMO.

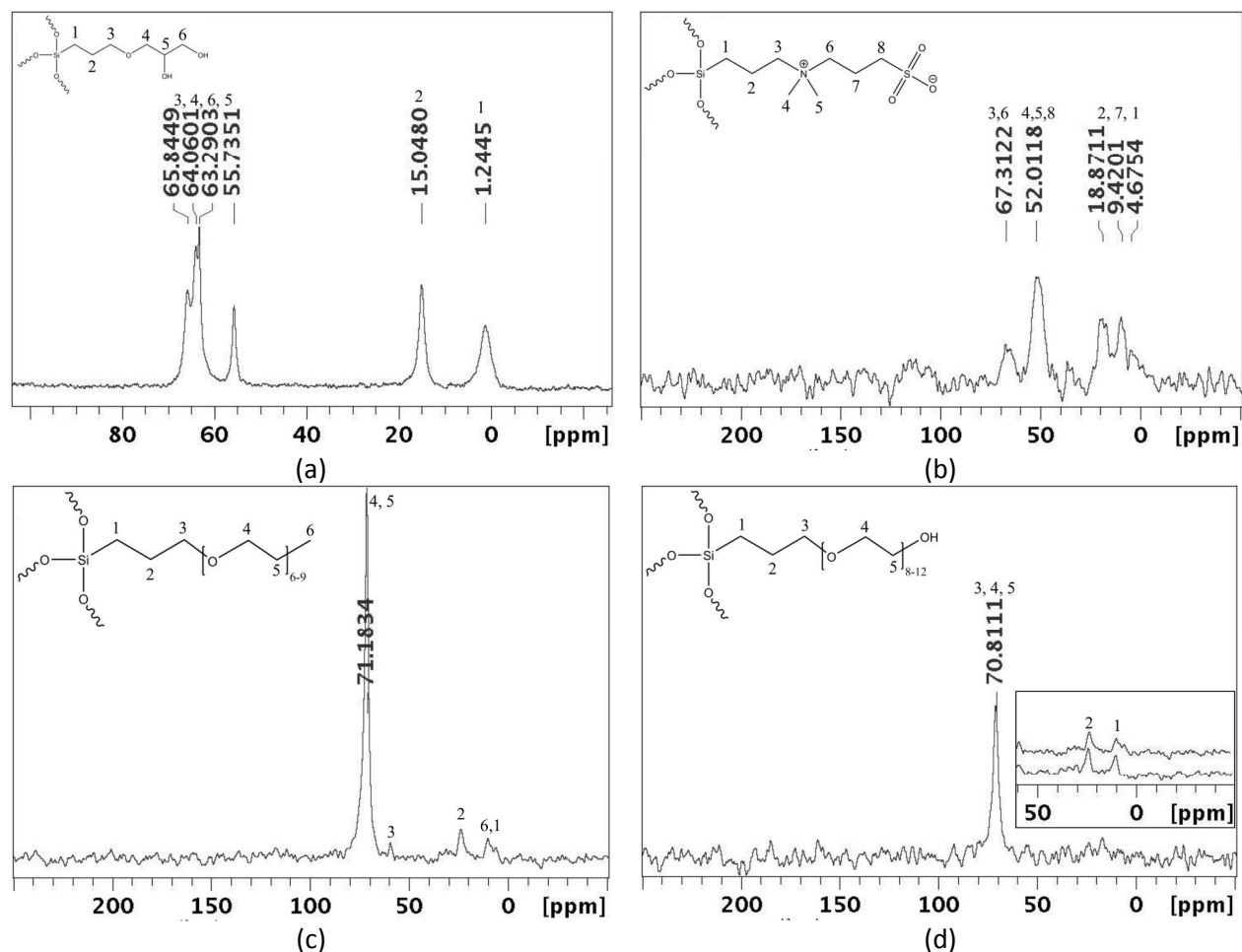


Figure 4. Solid-state ^{13}C (^1H) CP MAS NMR spectra with assignment of the carbon peaks for (a) NexSil6 + GLYMO, (b) NexSil6 + SB, (c) NexSil6+ PEG (6-9EO), and (d) ST-O + PEG (8-12 EO), Inset: reprocessed and smoothed data to accentuate peaks from carbon 1 and 2. Data in panel (a) were collected with a 4 mm MAS probe head and a 24 h total experimental time. Data in panels (b-d) were collected with a 2.5 mm MAS probe head and a 12 h total experimental time.

As shown in Figure 5, the zeta potential (ζ) of the bare silica particles with 10 mM added salt reaches a plateau value of ca. -40 mV at pH 9~11 and changes monotonically to approximately -5 mV at pH 3.5 as the silanols become more protonated, as expected.^{33, 69} With GLYMO and PEG (6-9EO) surface modification, the magnitude of the surface charge was lowered more at high pH values, where the initial magnitude of the charge was larger, than at low pH values. The changes were negligible in most cases for SB (consistent with previous results⁴) and PEG(8-12EO). The smaller change for SB and PEG(8-12EO) than for the others is consistent with a smaller fraction of a monolayer coverage, which left a large number of unmodified, charged silanol groups. Furthermore, the coverage of less than 40% of a monolayer in all of the cases also limited the change in ζ . For GLYMO, the change in ζ compared to the unmodified NPs is on the order of 5 to 10 mV from pH 9 to 4. For all ligands at pH 6 to 9, the significant

negative charge on the coated silica particles likely suggests a great propensity for monodentate or bidentate binding (Figure 1, lower), which are less effective at decreasing surface charge on silica particles than oligomerization.⁴

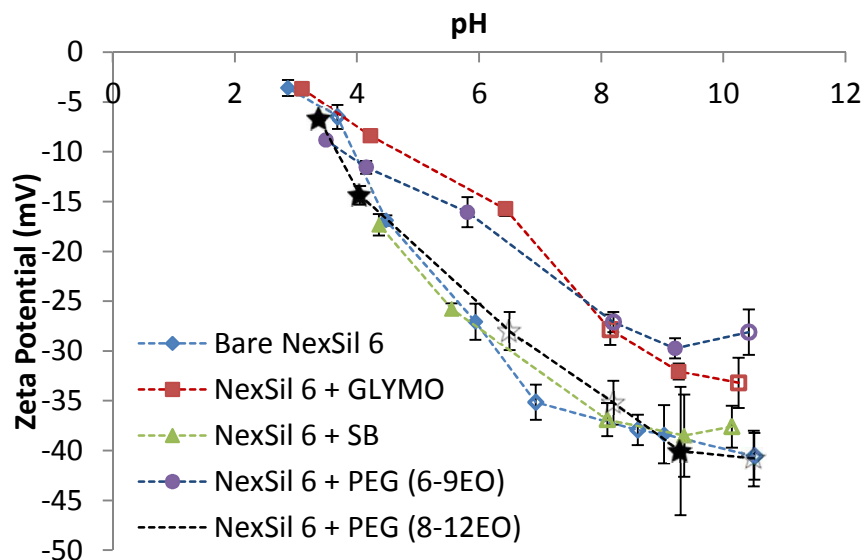


Figure 5. Zeta potential vs. pH of silica nanoparticles with 10 mM NaCl added, collected with Malvern Mastersizer (filled symbols) or 10 mM KCl added, collected with Brookhaven ZetaPALS (open symbols).

Stabilization of particles in high-salinity aqueous phases. Visual observations of NP dispersions were recorded up to 1 week in DI water or API brine at pH 8~9 (the unadjusted pH of the diluted NP dispersions) or pH 3.5 and are given in Table 2, and representative photographs are given in Figure S5. Remarkably, the GLYMO-coated particles appeared to be stable in that no visible settling (at the bottom of the vial) occurred for any sample condition tested. NexSil 6 NPs with SB only (denoted “NexSil 6 + SB”) were stable at pH 8, but rapidly aggregated when the pH of the dispersion was decreased below ca. pH 4.5. The reason for the loss of stability of SB-coated particles at low pH is to date unknown, but Muro et al.² also observed aggregation of sulfobetaine-coated quantum dots at pH 3, but not at higher pHs. Interestingly, after the SB NPs were further treated with GLYMO (denoted “NexSil 6 + SB**”), they no longer aggregated when the pH was decreased to 3.5, even though their organic fraction did not measurably increase during the second coating step (Table 1), indicating only a small amount of added GLYMO. Furthermore, the charge did not change measurably ($\zeta = -38.9 \pm 1.1$ mV at pH 8.95).

Table 2. Summary of stability observations up to 1 week via visual inspection in DI water or API brine.

Particle	pH 8~9 (unadjusted)		pH 3.5 (adjusted with HCl)		
	DI	API brine	DI	API brine	API brine (80°C)
NexSil 6 + GLYMO*	√	√	√	√	√
NexSil 6 + GLYMO	√	√	√	√	√
NexSil 12 + GLYMO	√	√	√	√	√
NexSil20 + GLYMO	√	√	√	√	√
NexSil125 + GLYMO	slight turbidity incr. in 2 days, no settling	slight turbidity incr. in 2 days, no settling	slight turbidity incr. in 2 days, no settling	slight turbidity incr. in 2 days, no settling	slight turbidity incr. in 2 days, no settling
ST-PS-S + GLYMO	√	√	√	turbidity incr. in 48h no settling	increased turbidity in 48h, no settling
ST-UP + GLYMO	√	√	√	√	√
NexSil 6 + SB	√	√	rapid aggregation below pH~4.5; settling in <1h	rapid aggregation below pH~4.5; settling in <1h	-
NexSil 6 + SB**	√	√	√	√	√
NexSil 6 + PEG (6-9EO)	√	√	√	√	rapid aggregation and settling at CFT
NexSil 6 + PEG (8-12EO)	√	√	√	√	rapid aggregation and settling at CFT

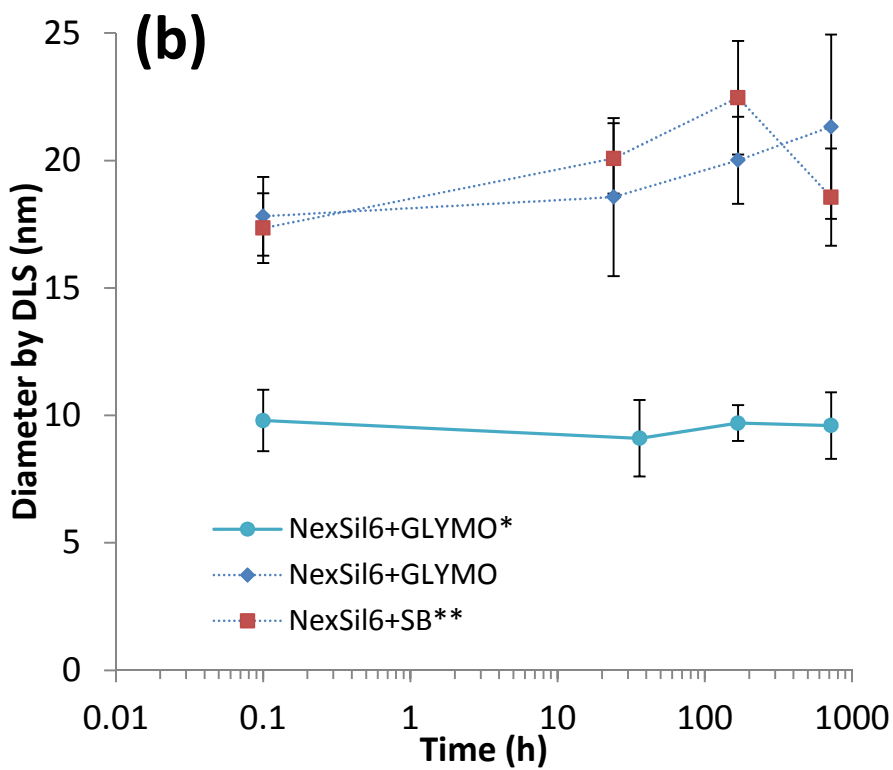
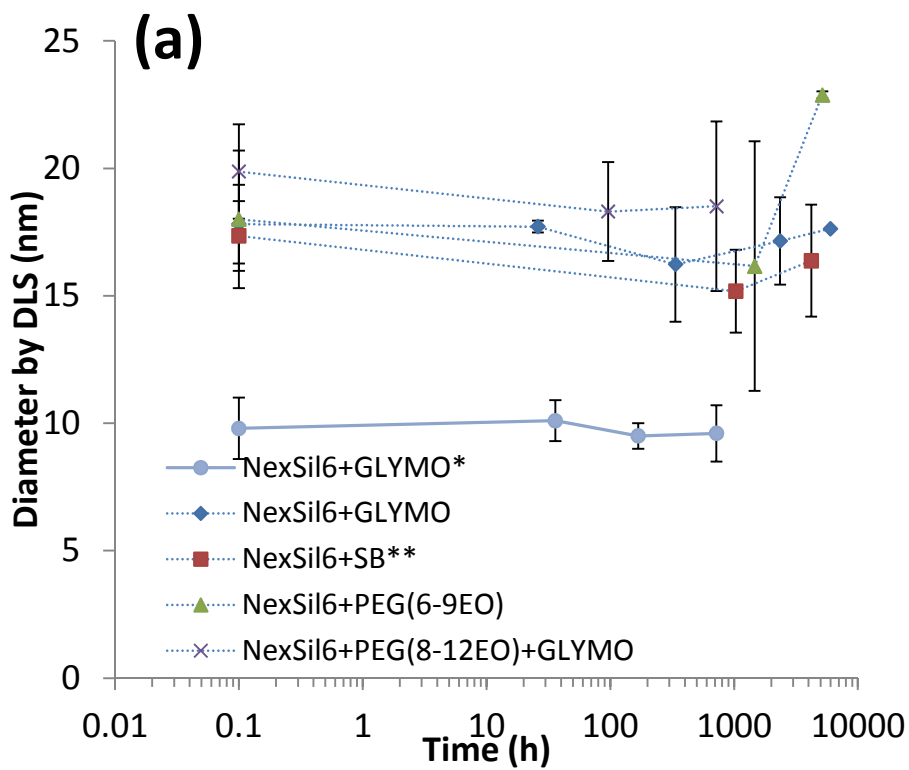
√=visually unchanged in 1 week

Both types of PEG-coated silica particles (6-9 or 8-12 EO groups) remained visually unchanged for 1 week at low temperature in pH 3.5 (adjusted with HCl) API brine. However, they both precipitated with a CFT of ~80°C in SSW. As the salinity was increased further in API brine, the CFT dropped as expected, on the basis of phase behavior of PEG,⁵⁴ to a value of ~50°C. This result is consistent with a previous report of 17 nm diameter silica NPs with grafted PEG(6-9) ligands which were stable against aggregation in 3 M NaCl at RT for 24 h, but rapidly aggregated when the temperature was increased to 37°C.⁵ In contrast, the ether diol in GLYMO stabilized the NPs in API brine to at least 120°C (Figure S7 and Table S5). The greater stabilization of the GLYMO-coated NPs could not be correlated to ligand phase behavior given that the ligands with either 6-9 or 8-12 EO groups were soluble in API brine at pH 7 up to 120°C over a wide range of ligand concentration (Figure S4). Instead, the greater stability of the GLYMO-coated particles may be attributed to: (1) the higher ligand coverage for the GLYMO-grafted than the PEG grafted NPs (Table 1), exposing fewer anionic silanol sites which may bridge with Ca²⁺ ions

and (2) lack of bridging interactions between the Ca^{2+} ions and the diol functionality in GLYMO relative to strong bridging with ether oxygens on the PEG chains.⁷⁰ It is not known why the second factor did not cause precipitation of the PEG oligomers ligands (without silica NPs) in API brine 120°C. Acting in conjunction with attractive interparticle vdW forces, the bridging attraction of Ca^{2+} to the anionic silanols and to PEG caused aggregation of the PEG-grafted NPs even though the PEG ligands were soluble at 120°C.

Interestingly, the aggregation of PEG(6-9EO)-coated particles appeared to be reversible, whereby the dispersion became transparent upon cooling (Figure S5e). Temperature responsive particles are often designed with coatings that demonstrate lower critical solution temperature (LCST) behavior.⁷¹⁻⁷³ For example, a similar reversible flocculation behavior was observed for gold NPs with bis(p-sulfonatophenyl)-phenylphosphine, where steric repulsion prevented the approach of NPs beyond ca. 0.5 nm.⁷¹

The visual observations presented above (Table 2) served as a guide for selecting conditions to further study systems with limited particle aggregation by measuring D_h vs. time data as shown in Figure 6. The results for particles with D_h less than 25 nm are given in Figures 6a-b and for larger NPs in Figure 6c. At room temperature in pH 3.5 API brine (Figures 6a and 6c), the D_h of all of the particles tested remained unchanged for the duration of the measurements (at least 30 days). At 80°C in API brine at pH 3.5, the smallest Nexsil 6 particles (shown in Figure 6b) remained unchanged in size while the larger NexSil 12- and NexSil 125-based particles (shown in Figure 6c) underwent slow aggregation. Additionally, ST-UP+GLYMO dispersions were aged at 80°C in pH 3.5 API brine for 110 days, and the average peak sizes were 80.3 ± 12.6 and 16.2 ± 0.6 , indicating no measurable aggregation. Despite the relatively strong vdW attraction between the large NexSil 125 particle cores,³⁶ the GLYMO provided steric stabilization at room temperature. A yellow color became present in the 0.5% N6+SB** sample after 2 months in API at 80°C (Figure S6). The cause of this change was unknown, given the high chemical stability of the sulfobetaine coating material.



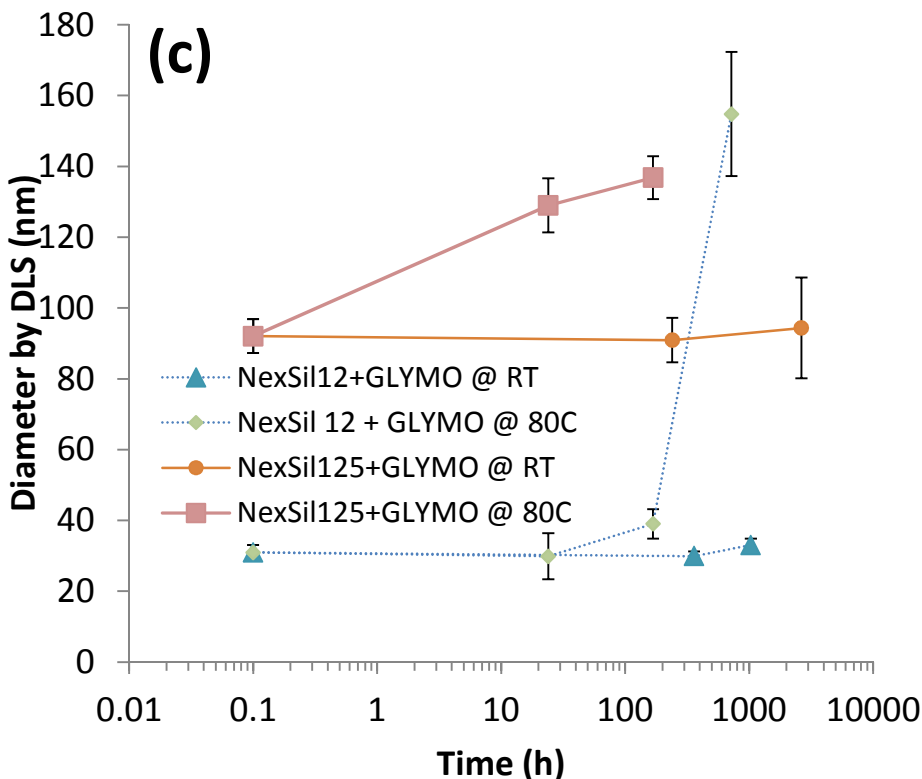


Figure 6. Nanoparticle stability via DLS measurements in pH 3.5 API brine for particles smaller than 25 nm at (a) RT and (b) 80°C, and (c) for larger particles at the temperature indicated in the legend. All experiments were at 0.5% w/v NPs. All data is tabulated in Table S3. Note that NexSil 125 + GLYMO @ 80°C aggregated to above 1 μm in less than 720 h (Table S4) whereas the remaining samples depicted in panels a-c remained colloidally stable.

To further examine the interactions between the nanoparticles, the rheology of a 5% NexSil 6 + GLYMO dispersion in API brine was determined (Figure 7). The very low viscosity (1.25 cP average between 1 and 100 s^{-1}) indicates the absence of gel formation^{12,14} that arises from the formation of fractal aggregates through attractive interactions such as vdW forces³² that produce a long-range structure.⁷⁴ At high concentrations of bare particles (e.g. at least 1.5% 5 nm diameter silica particles³¹) a single gel phase can form with high viscosities.^{31, 32, 74} Through grafting of GLYMO to the NP surfaces, attractive interactions that drive gel formation were strongly mitigated with steric repulsion, consistent with the lack of aggregation seen by DLS.

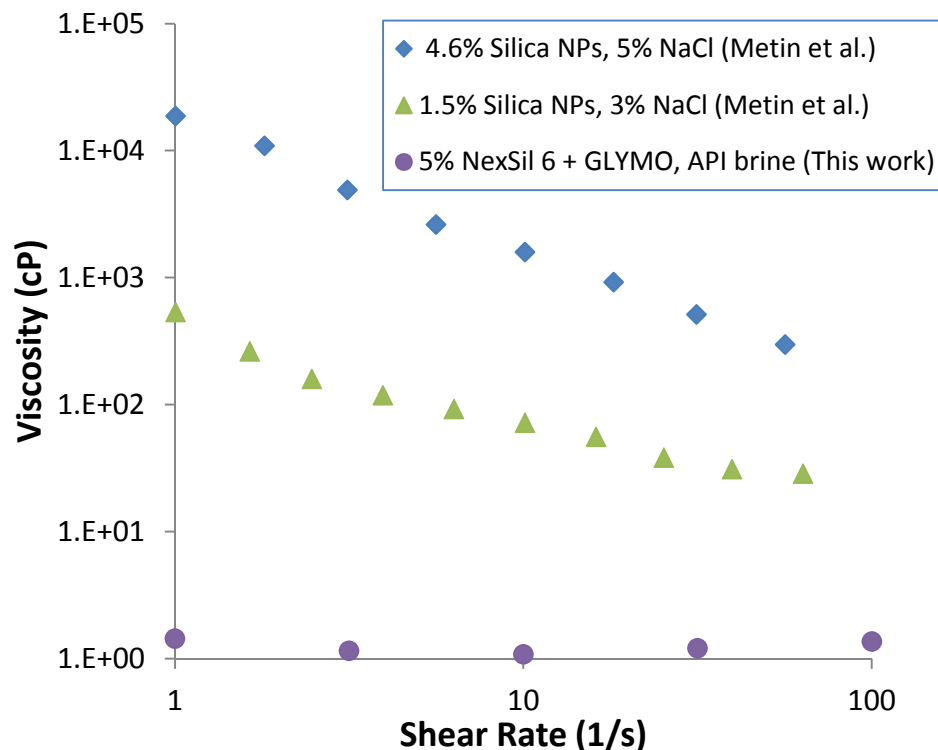


Figure 7. Steady-state shear rheology data collected for 5% w/v NexSil 6 + GLYMO in API brine at 25°C. Also plotted are data for aggregated silica particles given in Metin et al.³¹ The average viscosity from 1 to 100 s⁻¹ was 1.25 cP for the 5% NexSil 6 + GLYMO particles, 130 cP for the aggregated 1.5% silica NPs, and 4500 cP for the aggregated 4.6% silica NPs.

To further test the limits of stabilization, experiments were performed at higher temperatures and in even more concentrated brines. In “2xAPI brine” (16% NaCl + 4% CaCl₂) at room temperature and 80°C for NexSil 6 + GLYMO and NexSil 6 + SB** particles at pH 3.5 (adjusted with HCl and measured with a Mettler-Toledo FiveGo pH meter equipped with a micro pH probe) aggregation was not measurable by DLS in 2 days (Table S5). After 110 days, the dispersion of GLYMO-coated particles had decreased in volume by approximately 30% due to evaporation of water, leaving an unknown higher concentration of salts and NPs (Table S5). At this extreme condition, the D_h increased to ca. 50nm (Table S5), but no visible settling had occurred. At an extreme temperature of 120°C, NexSil 6 with GLYMO and SB** coatings were tested both pH 8-9 and 3.5 API brine for 3 days (Figure S7). Only the GLYMO-coated particles at pH 3.5 were stable enough for a DLS measurement, which indicated aggregation to ca. 50 nm (Table S5). At the other three conditions, massive aggregation and settling were observed (Figure S7a-c and Table S5).

Colloidal stability of slowly aggregating particles is often quantified by calculation of a stability ratio (W)^{25, 75} which was attempted as presented in the Supporting Information. However, given the extremes in colloidal stability (rapid aggregation above the CFT for PEG-coated particles or no measurable change in size for the most stable particles over at least 30 days) only upper or lower limits for W are provided in most cases. We note that the smallest and most stable particles (GLYMO- and SB**-coated) had a very high lower limit for W in API brine on the order of 10^{11} at both room temperature and 80°C (Table S6), in agreement with the remarkable stability of the particles.

To investigate the effect of GLYMO coverage on silica NPs, the initial GLYMO used in the grafted reaction was varied from 0.1 to 10 $\mu\text{mol}/\text{m}^2$. The resulting levels of GLYMO on the NP surfaces are given in Table 3 and Figure S8) along with the slightly different extents of aggregation during the grafting reaction (Figure S8b). Above a level of 5 $\mu\text{mol}/\text{m}^2$ of added GLYMO to the reaction, the NP surfaces become saturated at ca. 3 $\mu\text{mol}/\text{m}^2$, corresponding to ca. 38% of a monolayer (Figure S8a). The isotherm shown in Figure S8a is qualitatively similar to that given by Estephan and coworkers⁴ for SB on silica NPs, and both reach a saturation value near 5 $\mu\text{mol}/\text{m}^2$ of ligand added to the reaction. However, the saturation level of SB ligand added to silica particles was 1.7 $\mu\text{mol}/\text{m}^2$,⁴ indicating a more efficient grafting of GLYMO compared to SB.

Table 3. Summary of stability observations at 80°C up to 1 week via visual inspection for varying levels of grafting of GLYMO on the surface.

Resulting GLYMO on NP, $\mu\text{mol}/\text{m}^2$ (monolayer fraction)	pH 8~9 (unadjusted)			pH 3.5 (adjusted with HCl)		
	0.5% NaCl	SSW	API	0.5% NaCl	SSW	API
0.54 (7.1%)	XX	XX	XX	X	XX	XX
0.80 (11%)	v ⁺	XX	XX	X	X	XX
1.1 (15%)	v ⁺	XX	XX	0 ⁺	X	XX
2.0 (27%)	v ⁺	XX	XX	v ⁺	0	0 ⁺
2.8 (37%)	v ⁺	0 ⁺	X	v ⁺	v ⁺	v ⁺
2.9 (38%)	v ⁺	X	v ⁺	v ⁺	v ⁺	v ⁺

XX = aggregation and settling in < 1 day

X = aggregation and settling in 1-6 days

O = increased turbidity but no observable settling in 1 week

V = visually unchanged in 1 week

[†]DLS confirmed no aggregation in 1 week

[‡]DLS confirmed aggregation in 1 week

The variation of GLYMO ligand grafted to the silica particle surfaces resulted in a spectrum of colloidal behavior in the various aqueous solutions tested. In DI water (not shown), negligible changes in particle size were measured by DLS at 80°C up to 1 week in all cases (initial NP sizes are given in Figure S8b). When tested at higher salinity conditions (Table 3), particle stability was influenced by pH, brine concentration, and the GLYMO graft density. At the unadjusted pH of 8-9, particles with as little as 0.80 $\mu\text{mol}/\text{m}^2$ of GLYMO were stable in 0.5% NaCl. In SSW, however, none of the particles were completely resistant to aggregation at pH 8-9, but those with at least 2.8 $\mu\text{mol}/\text{m}^2$ of GLYMO did not visibly settle in the first 24h. We note that the SSW contains Mg^{2+} and Sr^{2+} in addition to Na^+ and Ca^{2+} , making it a more complicated system to interpret than API brine. In API brine, particles with the highest level of GLYMO coverage (2.9 $\mu\text{mol}/\text{m}^2$) did not undergo any measurable aggregation (by DLS) up to 1 week at either pH (indicated by a “[†]” in Table 3). In 0.5% NaCl, particles with a low GLYMO coverage of 0.80-1.1 $\mu\text{mol}/\text{m}^2$ were less stable at pH 3.5 compared to the same particles at pH 8-9. In pH adjusted SSW, the stability of particles with $\geq 0.80 \mu\text{mol}/\text{m}^2$ GLYMO was higher at pH 3.5 (added HCl) compared the same particles at pH 8-9. In API brine, the stability of particles with 2.0-2.8 $\mu\text{mol}/\text{m}^2$ GLYMO was also improved at pH 3.5. The behavior summarized in Table 3 suggests two regimes of colloidal stability at the lower GLYMO coverages before a requisite level of GLYMO was added such that the particles were stable at either pH: (1) in low salinity (and divalent-free) 0.5% NaCl, particles were more stable at higher pH, and (2) in higher salinity brine containing divalent cations, particles were more stable at lower pH.

Extended DLVO model to describe the colloidal stability

The calculated interaction potentials given in Figure 8 will now be used to demonstrate that GLYMO and SB, which are well-solvated, provide sufficient steric stabilization for colloidal stability. The molecular weight and ligand length used for the calculations were those of GLYMO (236 Da and 0.95 nm, respectively, Table S3), but the results for SB (molecular weight = 329.5 Da and length of 1.2 nm, Figure

S3) were similar semi-quantitatively to those for GLY MO and lead to identical conclusions. The van der Waals attraction (V_a) and electrostatic repulsion (V_r) are shown in Figure 8a-b for salinities from 0.01% NaCl to API brine. Note that only one V_a van der Waals curve is given because this potential is assumed to be independent of aqueous phase salinity. As salinity increases, significant reductions in V_r (Figure 8a) in API brine are very evident also in the total potential V_t shown in Figure 8b and particles would be unstable. The fact that the potential barrier completely disappears for API brine and not for SSW is likely due to the choice of a constant value of -35 mV for particle surface potential. In a real brine system, further reduction in surface potential due to cation-particle interactions may be expected.³³ Further destabilizing forces such as cation bridging of negative charges on the silica surface would be expected to destabilize particles at lower ionic strengths than those predicted solely by screened electrostatic repulsion.⁵¹ Bridging interactions with the negative charges on the silica surface may explain the lower stability of particles with low GLYMO coverages at high pH, where the surface charge of the silica particles is more negative (Figure 5). At lower pH, the surfaces become less negatively charged and the bridging interaction between the silica particle surface and cations in solution is reduced.³³ Higher amounts of grafted GLYMO remove ionizable silanol groups while adding nonionic alcohol groups which are less susceptible to interparticle Ca^{2+} bridging than ether oxygens in PEG oligomers.⁷⁰ In the case of SB-coated particles, the relatively weak interaction between Ca^{2+} ions and the sulfonate group compared to water-sulfonate group interactions prevented bridging attraction to the sulfonates.⁴² The small size of GLYMO or SB is likely sufficient to prevent bridging interactions to the remaining anions on the silica surface because the ligand is longer than the diameter of a hydrated Ca^{2+} ion (0.46-0.5 nm⁶⁶), effectively “burying” the deprotonated silanol surface charges.

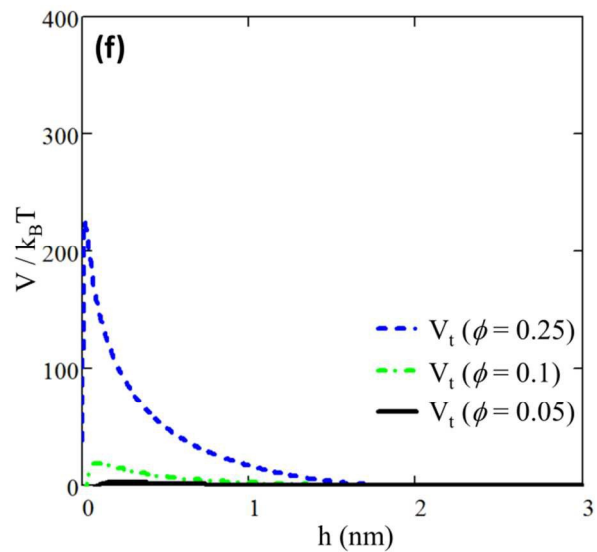
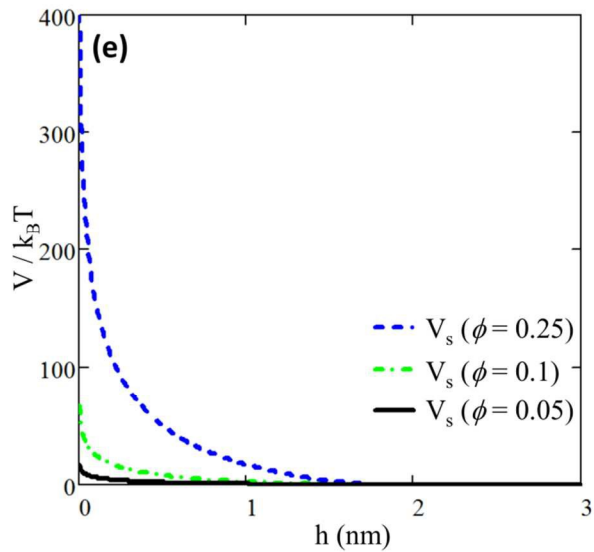
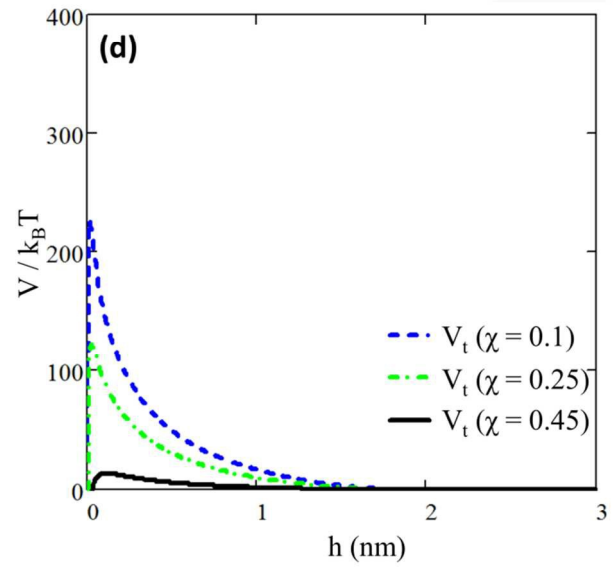
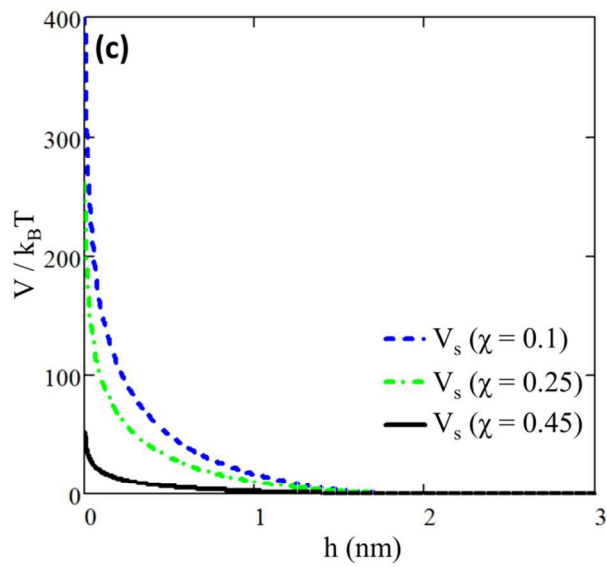
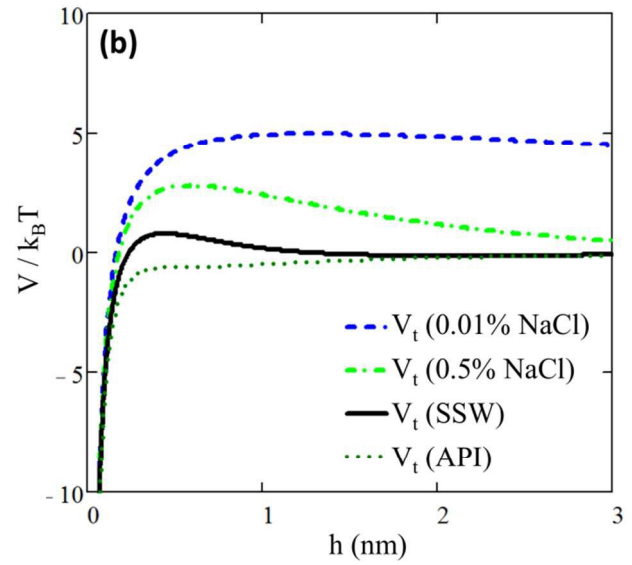
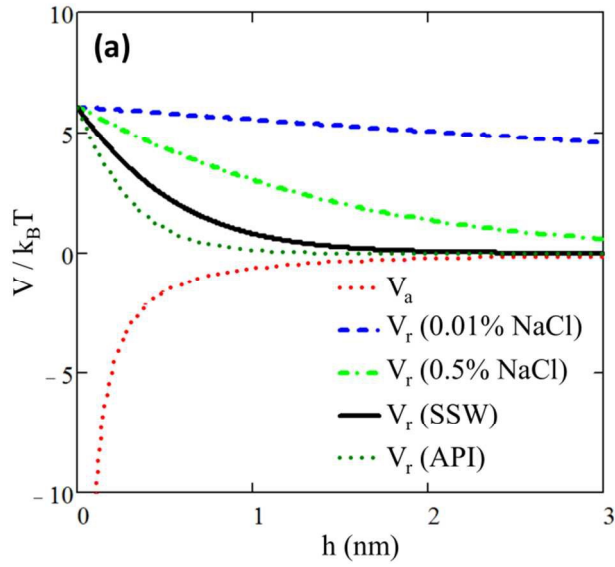


Figure 8. Interparticle interaction potential (V) for 16 nm diameter GLYMO-coated silica particle at pH 8 by extended DLVO calculations as a function of particle separation distance (h). (a) DLVO calculation of attractive van der Waals (V_a) potential (independent of salinity) and repulsive electrostatic (V_r) potentials in 0.01% NaCl, 0.5% NaCl, SSW, and API brine. (b) Total interaction potential (V_t) at the various salinities shown in panel (a). (c) Extended DLVO calculation of steric repulsion potential (V_s) at Flory-Huggins $\chi = 0.1, 0.25, \text{ and } 0.45$, holding the ligand volume fraction $\phi = 0.25$. (d) V_t in API brine including V_a and V_r shown in panel (a) as well as V_s shown in panel (c). (e) V_s at $\phi = 0.05, 0.1, \text{ and } 0.25$, holding $\chi = 0.1$. (f) V_t in API brine including V_a and V_r shown in panel (a) as well as V_s shown in panel (e).

Recently, molecular dynamics (MD) simulations have demonstrated that low concentrations of electrolytes (1.05×10^{-3} , 0.37×10^{-3} , and 0.06×10^{-3} mole fraction NaCl, CaCl₂, and MgCl₂, respectively, in an aqueous solution) may cause an electrical double layer to form even on neutrally charged silica surfaces.⁷⁶ The molar salt concentration at which the double layer formed was 3x higher in the case of NaCl (ca. 60 mM or 0.3 %w/v) than CaCl₂ (ca. 20 mM or 0.2 %w/v), in qualitative agreement with the order of salt effectiveness at causing particle destabilization. Nevertheless, thinning of the double layer was predicted at higher salt concentrations,⁷⁶ which leads to destabilization of the NPs above the CCC, in agreement with experimental results shown by Metin et al.⁷⁷ and in the present study.

For a ligand grafted to a NP surface, the solvation of the ligand plays an important role in the degree of steric stabilization.³⁶ The steric repulsion potentials (V_s) for $\chi = 0.1$ (well solvated), $\chi = 0.25$ (intermediate), and $\chi = 0.45$ (weakly solvated) are shown in Figure 8c for a constant ligand volume fraction of 0.25 in the coating layer. In all cases, the range of repulsion is roughly twice the ligand length, but the magnitude of repulsion is highly dependent on the χ parameter. The combination of V_a and V_r calculated for API brine from Figure 8a with V_s gives the V_t as shown in Figure 8d. Even for a χ of 0.25, the barrier is large, >100 kT, indicating the dominant role of steric stabilization that prevents close separation distances where VDW forces would otherwise cause aggregation. Solubility of GLYMO in API brine up to 120°C suggested a $\chi < 0.5$ at lower temperatures such as 80°C, in agreement with the extended DLVO results which indicate that it had a sufficiently low χ to provide significant steric repulsion for a repulsive V_t in API brine at 80°C as seen in the experimental results. For a poor solvent when $\chi = 0.5$ (not shown), the ligands no longer provide repulsion, and when $\chi > 0.5$ (where the pure ligands would phase separate from the aqueous phase) the interparticle ligand attraction would destabilize the particles. For example, modification of silica NPs with hydrophobic ligands such as methyl-silanes causes destabilization in aqueous media.⁷⁸

The phase behavior of particles shown in Table 3 indicated a spectrum of behavior with different GLYMO coverages. To characterize this phenomena, V_s was calculated with ϕ values of 0.05 (very low coverage) to 0.1 (moderate coverage) to 0.25 (high coverage) at a constant $\chi = 0.1$ (indicating a well-solvated ligand). At the lowest coverage, the repulsion provided by the ligands was insufficient to overcome V_a . At high ligand coverages with a well-solvated ligand, the V_t peaks at over 200 $k_B T$, indicating high stability is possible with a low molecular weight ligand like GLYMO. It is likely that this potential would still be very large even when bridging attraction is included. The calculated V_s values are similar to those calculated by Wijenayaka and coworkers⁶⁵ for 13 nm gold NPs coated with 6-mercaptophexanoic acid at low salinities (MW = 148.22).

Applications of NPs stable in high salinity brine

Stability of particles in extremely high salinity brines such as seawater or oil reservoir brine is of interest for many applications in environmental science. In enhanced oil recovery (EOR), particles must remain small and unaggregated to undergo transport through pores that range in size from tens of nm to a few μm . In particular, some polymer-coated NPs have received attention for EOR applications due to their high stability in brine.²³ However, low molecular weight coatings offer the advantage of using (1) less and/or (2) a lower cost material to stabilize particles. For example, in this study we demonstrate large ca. 100 nm particles which are stable in API brine at room temperature for over 30 days (Figure 6c) using only 3.1% organic material (GLYMO). Similarly sized iron oxide particles require 20-40% added polymer to have equivalent stability.^{18, 42}

The understanding of particle stabilization with low molecular weight ligands in this study is relevant for the design of stable CO_2 -in-water (C/W) foams for EOR applications. For example, silica particles modified with dimethyl ligands have been used to generate C/W foams, but these particles were not stable at salinities at even 1% NaCl due to the hydrophobic nature of the ligands.⁷⁸ Silica particles coated with a "short chain" PEG ligand stabilized C/W foams in API brine at up to 50°C,⁷⁹ but neither the detailed structure of the ligand nor stability of the particles were provided. Additionally, silica particles with an unknown coating were tested in SSW for C/W foam generation at 50°C, but again no detail on the ligand structure was given.⁷⁹ Overall, there is a great need for further interfacial characterization of NPs with low molecular weight ligands in brine, which will be the subject of future studies.

Conclusions

Silica nanoparticles have been stabilized sterically against aggregation in seawater and even more concentrated brines containing divalent cations by grafting low molecular weight ligands (<600 g/mol) including an ether diol (GLYMO), PEG oligomers, and a zwitterionic sulfobetaine (SB). This elusive goal was achieved by identifying four types of highly solvated ligands that were soluble at 120°C in API brine (8% NaCl + 2% CaCl₂) and thus predisposed to functioning as steric stabilizers, according to the concept of Napper.³⁶ Whereas stabilization in API brine was achieved at room temperature at pH 3.5 for 7.4 nm NPs with all of the ligands, only GLYMO and SB ligands were successful up to 80°C for over 30 days in pH 3.5 API brine. Moreover, GLYMO provided colloidal stability for three days even at 120°C. An extended DLVO model signifies the steric stabilization is strongly dominant against van der Waals attraction for ~10 nm particles for these solvated ligands. Furthermore, because GLYMO and SB ligands are longer than the diameter of a Ca²⁺ ion, they “bury” residual unmodified charged deprotonated silanol groups on the particle surfaces to mitigate bridging attraction with divalent cations. In contrast PEG ligands were only effective stabilizers up to ~50°C in API brine, despite their solubility at 120°C, perhaps because of well-known bridging interactions between the ether oxygens and divalent cations. The ability to sterically stabilize NPs in concentrated electrolytes, including divalent ions, by grafting low MW ligands with simple silylation chemistry may find great interest in a variety of subsurface energy, biomedical, environmental, and oceanic applications over a wide range of temperature.

Supporting Information

Calculation methodology for ligand coverage on NPs, additional details of the DLVO calculations, characterization of ligand solubility in brine, additional images of NP dispersions, tables of data shown in Figure 6, calculation of stability ratio *W*, and additional information on the effect of varying GLYMO coverage on NPs. This material is available free of charge via the Internet at <http://pubs.acs.org>.

Corresponding Author

* E-mail: kpj@che.utexas.edu

Notes

The authors declare no competing financial interest.

Acknowledgements

The authors thank Vladimir Bakhmoutov and Greg Wylie for NMR measurements and assistance in interpretation of data; Hugo Celio for assistance with TGA; Dwight Romanovicz, Robert Stover, and

Joseph Schroer for assistance with and collection of TEM images; John Southwell for assistance with the BET method; William Hardin and Jefferson Liu for BET measurements; Muhammad Iqbal for zeta potential measurements; and Kishore Mohanty for use of the rheometer. This work was supported in part by the Gulf of Mexico Research Initiative and the DOE Center for Frontiers of Subsurface Energy Security. KPJ and TMT also acknowledge the Robert A. Welch Foundation (F-1319 and F-1696, respectively).

References

1. J. B. Schlenoff, *Langmuir*, 2014, **30**, 9625-9636.
2. E. Muro, T. Pons, N. Lequeux, A. Fragola, N. Sanson, Z. Lenkei and B. Dubertret, *Journal of the American Chemical Society*, 2010, **132**, 4556-4557.
3. S. Jiang and Z. Cao, *Advanced Materials*, 2010, **22**, 920-932.
4. Z. G. Estephan, J. A. Jaber and J. B. Schlenoff, *Langmuir*, 2010, **26**, 16884-16889.
5. Z. G. Estephan, P. S. Schlenoff and J. B. Schlenoff, *Langmuir*, 2011, **27**, 6794-6800.
6. M. G. Elimelech, J.; Jia, X. , *Particle deposition and aggregation: measurement, modelling and simulation*, Butterworth-Heinemann, 2013.
7. N. Saleh, T. Phenrat, K. Sirk, B. Dufour, J. Ok, T. Sarbu, K. Matyjaszewski, R. D. Tilton and G. V. Lowry, *Nano Letters*, 2005, **5**, 2489-2494.
8. A. A. Keller, H. Wang, D. Zhou, H. S. Lenihan, G. Cherr, B. J. Cardinale, R. Miller and Z. Ji, *Environmental Science & Technology*, 2010, **44**, 1962-1967.
9. V. K. Sharma, K. M. Siskova, R. Zboril and J. L. Gardea-Torresdey, *Advances in Colloid and Interface Science*, 2014, **204**, 15-34.
10. A. J. Worthen, L. M. Foster, J. Dong, J. A. Bollinger, A. H. Peterman, L. E. Pastora, S. L. Bryant, T. M. Truskett, C. W. Bielawski and K. P. Johnston, *Langmuir*, 2014, **30**, 984-994.
11. D. Kim and R. Krishnamoorti, *Industrial & Engineering Chemistry Research*, 2015, **54**, 3648-3656.
12. H. G. Bagaria, Z. Xue, B. M. Neilson, A. J. Worthen, K. Y. Yoon, S. Nayak, V. Cheng, J. H. Lee, C. W. Bielawski and K. P. Johnston, *ACS Applied Materials & Interfaces*, 2013, **5**, 3329-3339.
13. J. M. Berlin, J. Yu, W. Lu, E. E. Walsh, L. Zhang, P. Zhang, W. Chen, A. T. Kan, M. S. Wong, M. B. Tomson and J. M. Tour, *Energy & Environmental Science*, 2011, **4**, 505-509.
14. D. T. Wasan and A. D. Nikolov, *Nature*, 2003, **423**, 156-159.
15. A. Ditsch, P. E. Laibinis, D. I. C. Wang and T. A. Hatton, *Langmuir*, 2005, **21**, 6006-6018.
16. M. Ranka, P. Brown and T. A. Hatton, *ACS Applied Materials & Interfaces*, 2015, **7**, 19651-19658.
17. D. Wasan, A. Nikolov and K. Kondiparty, *Current Opinion in Colloid & Interface Science*, 2011, **16**, 344-349.
18. H. G. Bagaria, K. Y. Yoon, B. M. Neilson, V. Cheng, J. H. Lee, A. J. Worthen, Z. Xue, C. Huh, S. L. Bryant, C. W. Bielawski and K. P. Johnston, *Langmuir*, 2013, **29**, 3195-3206.
19. H. G. Bagaria, B. M. Neilson, A. J. Worthen, Z. Xue, K. Y. Yoon, V. Cheng, J. H. Lee, S. Velagala, C. Huh, S. L. Bryant, C. W. Bielawski and K. P. Johnston, *Journal of Colloid and Interface Science*, 2013, **398**, 217-226.
20. A. Chengara, A. D. Nikolov, D. T. Wasan, A. Trokhymchuk and D. Henderson, *Journal of Colloid and Interface Science*, 2004, **280**, 192-201.
21. A. J. Worthen, H. G. Bagaria, Y. Chen, S. L. Bryant, C. Huh and K. P. Johnston, *Journal of Colloid and Interface Science*, 2013, **391**, 142-151.
22. A. J. Worthen, S. L. Bryant, C. Huh and K. P. Johnston, *AIChE Journal*, 2013, **59**, 3490-3501.
23. H. ShamsiJazeyi, C. A. Miller, M. S. Wong, J. M. Tour and R. Verduzco, *Journal of Applied Polymer Science*, 2014, **131**, n/a-n/a.
24. Y. Chen, A. S. Elhag, B. M. Poon, L. Cui, K. Ma, S. Y. Liao, P. P. Reddy, A. J. Worthen, G. J. Hirasaki and Q. P. Nguyen, *SPE Journal*, 2013, **19**, 249-259.
25. P. Hiemenz, C. and R. Rajagopalan, *Principles of Colloid and Surface Chemistry*, Taylor & Francis Group, LLC, Boca Raton, FL, Third edn., 1997.
26. W. P. Wuelfing, F. P. Zamborini, A. C. Templeton, X. Wen, H. Yoon and R. W. Murray, *Chemistry of Materials*, 2001, **13**, 87-95.

27. F. P. Zamborini, J. F. Hicks and R. W. Murray, *Journal of the American Chemical Society*, 2000, **122**, 4514-4515.
28. P. C. Hiemenz and R. Rajagopalan, *Principles of Colloid and Surface Chemistry*, Marcel Dekker, inc., New York, 3 edn., 1997.
29. J.-P. Hsu and Y.-C. Kuo, *Journal of Colloid and Interface Science*, 1997, **185**, 530-537.
30. A. Amiri, G. Øye and J. Sjöblom, *Colloids and Surfaces A: Physicochemical and Engineering Aspects*, 2009, **349**, 43-54.
31. C. Metin, K. Rankin and Q. Nguyen, *Appl Nanosci*, 2012, 1-9.
32. C. Metin, R. Bonnacaze, L. Lake, C. Miranda and Q. Nguyen, *Appl Nanosci*, 2012, 1-10.
33. L. H. Allen and E. Matijević, *Journal of Colloid and Interface Science*, 1969, **31**, 287-296.
34. M. Baalousha, Y. Nur, I. Römer, M. Tejamaya and J. R. Lead, *Sci. Total Environ.*, 2013, **454-455**, 119-131.
35. K. A. Huynh and K. L. Chen, *Environ. Sci. Technol.*, 2011, **45**, 5564-5571.
36. D. H. Napper, *Polymeric Stabilization of Colloidal Dispersions*, Academic Press, New York, 1983.
37. K. J. Ziegler, R. C. Doty, K. P. Johnston and B. A. Korgel, *J. Am. Chem. Soc.*, 2001, **123**, 7797-7803.
38. G. C. Kini, J. Yu, L. Wang, A. T. Kan, S. L. Biswal, J. M. Tour, M. B. Tomson and M. S. Wong, *Colloid Surface A*, 2014, **443**, 492-500.
39. K. Y. Yoon, Z. Li, B. M. Neilson, W. Lee, C. Huh, S. L. Bryant, C. W. Bielawski and K. P. Johnston, *Macromolecules*, 2012, **45**, 5157-5166.
40. M. J. Kadhum, D. P. Swatske, J. H. Harwell, B. Shiau and D. E. Resasco, *Energy & Fuels*, 2013, **27**, 6518-6527.
41. Y. G. Wang, M. D. Becker, V. L. Colvin, L. M. Abriola and K. D. Pennell, *Environmental Science & Technology*, 2014, **48**, 10664-10671.
42. E. L. Foster, Z. Xue, C. M. Roach, E. S. Larsen, C. W. Bielawski and K. P. Johnston, *ACS Macro Letters*, 2014, **3**, 867-871.
43. Y. C. Park, J. Paulsen, R. J. Nap, R. D. Whitaker, V. Mathiyazhagan, Y. Q. Song, M. Hurlimann, I. Szleifer and J. Y. Wong, *Langmuir*, 2014, **30**, 784-792.
44. Y. Park, R. D. Whitaker, R. J. Nap, J. L. Paulsen, V. Mathiyazhagan, L. H. Doerrer, Y.-Q. Song, M. D. Huerlimann, I. Szleifer and J. Y. Wong, *Langmuir*, 2012, **28**, 6246-6255.
45. Q. Zhao, N. Chen, D. Zhao and X. Lu, *ACS Applied Materials & Interfaces*, 2013, **5**, 11453-11461.
46. K. Doiron, E. Pelletier and K. Lemarchand, *Aquatic Toxicology*, 2012, **124-125**, 22-27.
47. R. J. Nap, S. H. Park and I. Szleifer, *Journal of Polymer Science Part B: Polymer Physics*, 2014, **52**, 1689-1699.
48. Z. Xue, E. Foster, Y. Wang, S. Nayak, V. Cheng, V. W. Ngo, K. D. Pennell, C. W. Bielawski and K. P. Johnston, *Energy & Fuels*, 2014, **28**, 3655-3665.
49. R. J. Nap, S. H. Park and I. Szleifer, *Journal of Polymer Science Part B-Polymer Physics*, 2014, **52**, 1689-1699.
50. E. Katz and I. Willner, *Angewandte Chemie International Edition*, 2004, **43**, 6042-6108.
51. D. Wang, B. Tejerina, I. Lagzi, B. Kowalczyk and B. A. Grzybowski, *ACS Nano*, 2011, **5**, 530-536.
52. H. Wei, N. Insin, J. Lee, H.-S. Han, J. M. Cordero, W. Liu and M. G. Bawendi, *Nano Letters*, 2012, **12**, 22-25.
53. L. L. Rouhana, J. A. Jaber and J. B. Schlenoff, *Langmuir*, 2007, **23**, 12799-12801.
54. S. Nozary, H. Modarress and A. Eliassi, *Journal of Applied Polymer Science*, 2003, **89**, 1983-1990.
55. Y. C. Bae, S. M. Lambert, D. S. Soane and J. M. Prausnitz, *Macromolecules*, 1991, **24**, 4403-4407.
56. J. H. Heo, H. H. Cho and J. H. Lee, *Analyst*, 2014, **139**, 5936-5944.
57. A. B. Bourlinos, A. Stassinopoulos, D. Anglos, R. Zboril, M. Karakassides and E. P. Giannelis, *Small*, 2008, **4**, 455-458.
58. X. Yang and Z.-h. Liu, *Nanoscale Res Lett*, 2010, **5**, 1324-1328.

59. M. Templin, U. Wiesner and H. W. Spiess, *Advanced Materials*, 1997, **9**, 814-817.
60. H. E. Bergna, in *Colloidal Silica: Fundamentals and Applications*, eds. H. E. Bergna and W. O. Roberts, CRC Press, Boca Raton, 2006, vol. 131, p. 9.
61. S. R. Raghavan, J. Hou, G. L. Baker and S. A. Khan, *Langmuir*, 2000, **16**, 1066-1077.
62. T. López-León, A. B. Jódar-Reyes, D. Bastos-González and J. L. Ortega-Vinuesa, *The Journal of Physical Chemistry B*, 2003, **107**, 5696-5708.
63. B. Vincent, J. Edwards, S. Emmett and A. Jones, *Colloids and Surfaces*, 1986, **18**, 261-281.
64. G. Fritz, V. Schädler, N. Willenbacher and N. J. Wagner, *Langmuir*, 2002, **18**, 6381-6390.
65. L. A. Wijenayaka, M. R. Ivanov, C. M. Cheatum and A. J. Haes, *The Journal of Physical Chemistry C*, 2015, **119**, 10064-10075.
66. C. A. Silvera Batista, R. G. Larson and N. A. Kotov, *Science*, 2015, **350**.
67. S. P. Christensen, F. A. Donate, T. C. Frank, R. J. LaTulip and L. C. Wilson, *Journal of Chemical & Engineering Data*, 2005, **50**, 869-877.
68. B. N. Khlebtsov and N. G. Khlebtsov, *Colloid J*, 2011, **73**, 118-127.
69. G. Xu, J. Zhang and G. Song, *Powder Technology*, 2003, **134**, 218-222.
70. E. Beaudoin, C. Gourier, R. C. Hiorns and J. François, *Journal of Colloid and Interface Science*, 2002, **251**, 398-408.
71. Y. Liu, X. Han, L. He and Y. Yin, *Angewandte Chemie International Edition*, 2012, **51**, 6373-6377.
72. C. Durand-Gasselín, M. Capelot, N. Sanson and N. Lequeux, *Langmuir*, 2010, **26**, 12321-12329.
73. T. Saigal, H. Dong, K. Matyjaszewski and R. D. Tilton, *Langmuir*, 2010, **26**, 15200-15209.
74. D. Senis and C. Allain, *Physical Review E*, 1997, **55**, 7797-7800.
75. J. Dong, S. Chen, D. S. Corti, E. I. Franses, Y. Zhao, H. T. Ng and E. Hanson, *Journal of Colloid and Interface Science*, 2011, **362**, 33-41.
76. S. d. L. Lucas, A. R. Vagner, F. M. Mateus, O. M. Cigdem, P. N. Quoc and R. M. Caetano, *Journal of Physics: Condensed Matter*, 2015, **27**, 325101.
77. C. Metin, L. Lake, C. Miranda and Q. Nguyen, *J Nanopart Res*, 2011, **13**, 839-850.
78. B. P. Binks, B. Duncumb and R. Murakami, *Langmuir*, 2007, **23**, 9143-9146.
79. A. Aroonsri, A. J. Worthen, T. Hariz, K. P. Johnston, C. Huh and S. L. Bryant, *SPE 166319*, presented at SPE ATCE, New Orleans, LA, Sept. 30-Oct. 2., 2013.